Original scientific paper
https://doi.org/10.33180/InfMIDEM2025.302

Informacije MIDEM
Journal of Microelectronics,
Electronic Components and Materials
Vol. 55, No. 3(2025), 151 – 165

# *Microcontroller Realization of a Novel 4D Hyperchaotic System and Its Autonomous Mobile Robot Application*

*Betül Yürdem, Mustafa Furkan Aksu, Mehmet Sağbaş*

*Department of Electrical and Electronics Engineering, Izmir Bakircay University, Menemen, İzmir, Turkey.*

**Abstract:** The chaotic systems offer benefits in diverse domains, including encryption and communication systems, particularly in the upkeep of intricate and safeguarded systems. This study introduces a new hyperchaotic system with four dimensions (4D), seven parameters, and four quadratic non-linear terms. An extensive analysis is conducted on the suggested hyperchaotic system to investigate its dynamic properties, such as chaotic attractors, stability of equilibrium points, spectrum of Lyapunov exponents (LE), bifurcation diagram, etc. The proposed system is validated both by experimental tests using an embedded hardware STM32 microcontroller and MATLAB simulations. The microcontroller-based chaotic systems proposed in the literature and the given hyperchaotic system in this study are compared in a tabular form. The outcomes of these trials constantly correspond, offering theoretical validation for the utilization of this hyperchaotic system in real-world applications. An application example of an autonomous mobile robot (AMR) driven by the presented hyperchaotic system is provided in this work, as efficient and fast terrain exploration is a crucial problem in AMR path planning research.

**Keywords:** chaos; hyperchaotic systems; embedded systems; microcontroller-based implementation; Autonomous mobile robots; chaotic path planning

# *Mikrokrmilniška realizacija novega 4D hiperkaotskega sistema in njegova avtonomna uporaba za mobilne robote*

**Izvleček:** Kaotični sistemi so koristni na različnih področjih, vključno s šifrirnimi in komunikacijskimi sistemi, zlasti pri vzdrževanju zapletenih in zaščitenih sistemov. Ta študija uvaja nov hiperkaotični sistem s štirimi dimenzijami (4D), sedmimi parametri in štirimi kvadratnimi nelinearnimi členi. Na predlaganem hiperkaotičnem sistemu je opravljena obsežna analiza, da bi raziskali njegove dinamične lastnosti, kot so kaotični atraktorji, stabilnost ravnovesnih točk, spekter Ljapunovovih eksponentov (LE), bifurkacijski diagram itd. Predlagani sistem je potrjen z eksperimentalnimi preskusi z vgrajenim strojnim mikrokrmilnikom STM32 in simulacijami v programu MATLAB. V literaturi predlagani kaotični sistemi, ki temeljijo na mikrokrmilnikih, in dani hiperkaotični sistem v tej študiji so primerjani v obliki tabele. Rezultati teh poskusov se dobro ujemajo, kar ponuja teoretično potrditev uporabe tega hiperkaotičnega sistema v realnih aplikacijah. V članku je podan primer uporabe avtonomnega mobilnega robota (AMR), ki ga poganja predstavljeni hiperkaotični sistem, saj je učinkovito in hitro raziskovanje terena ključni problem pri raziskavah načrtovanja poti AMR.

**Ključne besede:** kaos; hiperkaotični sistemi; vgrajeni sistemi; implementacija na osnovi mikrokrmilnika; avtonomni mobilni roboti; kaotično načrtovanje poti

** Corresponding Author's e-mail: mehmet.sagbas@bakircay.edu.tr*

How to cite:
B. Yürdem et al., "Microcontroller Realization of a Novel 4D Hyperchaotic System and Its Autonomous Mobile Robot Application", Inf. Midem-J. Microelectron. Electron. Compon. Mater., Vol. 55, No. 3(2025), pp. 151–165

## 1 Introduction

Chaos theory unveils the fascinating duality of complex systems: governed by deterministic equations yet exhibiting seemingly random and unpredictable behavior. This paradoxical blend, aptly described as a "completely predictable state of confusion" [1], lies at the heart of numerous natural and engineered phenomena. Its study sheds light on diverse systems, ranging from weather patterns and ecological dynamics to population fluctuations and economic models [2 – 4]. Rossler conducted the initial research on the notion of hyperchaos [5]. The number of positive LE in the system frequently determines how complex the chaotic behavior of these systems is. Systems with one or more positive LE are considered chaotic, whereas those with two or more are considered hyperchaotic.

4D hyperchaotic systems belong to a fascinating class of complex systems. These systems are highly sensitive to initial circumstances and display complex dynamics, resulting in butterfly effects where small variations in the starting point can cause significantly different and unforeseen consequences [6]. This very sensitivity, however, allows for potential control and manipulation, making them alluring objects of research for engineers and mathematicians alike [6, 7]. An increasing number of researchers have started looking for chaotic systems with more sophisticated dynamic behaviors to increase the security of chaotic information encryption and chaotic secure communication [8 – 10].

In recent times, there has been a proliferation of proposed hyperchaotic systems that have gained extensive utilization across various domains such as information processing, neuroscience, electronics, communications, and information technology [11] – [28]. Their more intricate dynamics have facilitated the development of secure communication, audio encryption, video encryption, and image encryption.

A 4D autonomous chaotic system with cubic nonlinear terms in each equation is presented in [11]. The given system can produce complex dynamics over a wide range of parameter values, such as chaos, period doubling bifurcation, Hopf bifurcation, periodic orbit, source, sink, and so forth. The study in [12] delves into a novel 4D chaotic system built on cubic non-linear terms. The proposed system exhibits two double-wing chaotic attractors that exist simultaneously. In Ref [13], an efficient method to design S-boxes based on the Qi Hyperchaos System is proposed. It is aimed at creating more robust S-boxes that can provide diffusion and confusion properties together.

A new hyperchaotic attractor has been proposed by combining a uniform flux-controlled memristor and a cross-product term to the 3D autonomous chaotic system [14]. In the study conducted in [15], a 4D chaotic system includes four non-linear terms and four variable parameters. In [16], a hyperchaotic system with a butterfly effect is given. Numerical simulations and circuit implementation investigate the system's fundamental dynamic properties.

Embedded hardware such as Field Programmable Gate Arrays (FPGAs) are widely used to simulate and control hyperchaotic systems [17] – [20]. A five-dimensional (5D) hyperchaotic system is presented and realized in FPGA [17]. It has an exponential-term and memristive model. The fundamental properties are examined using bifurcation diagrams, phase diagrams, and the LE. 4D and 5D hyperchaotic systems based on the classical Sprott-C three-dimensional (3D) system are presented in [18]. The proposed systems were realized by an FPGA and demonstrated by an experimental result. The main characteristics of the proposed system are demonstrated using LE spectra, phase diagrams, and bifurcation diagrams. A multistable 4D hyperchaotic system is implemented using an FPGA and a MultiSim circuit simulator in [19]. The fundamental characteristics of the suggested system are also analyzed. In [20], a 4D hyperchaotic system is proposed. There are two nonlinear terms among the nine terms in the presented system's dynamics. Additionally, the system exhibits multistability behavior within a certain range. Phase plots, Lyapunov spectra, Kaplan-Yorke dimension, and bifurcation diagrams are utilized to examine the system's intricate dynamic behavior. The implementation of FPGA is also realized.

Real-time capabilities, low costs, power consumption, connectivity, and digital signal processing all contribute to the STM32's widespread use in numerous industries, including communications, industrial automation, control, and the Internet of Things (IoT) [21] – [26]. Some researchers have worked on the realization of chaotic systems using microcontrollers such as Arduino, STM32, PIC18F, etc.

Based on a 3D Lü chaotic system, a 4D hyperchaotic system is built in [21]. The properties of the presented system, including chaotic attractors, the spectrum of LE, equilibrium point stability, and the bifurcation diagram, are investigated. Experimental validation is performed on STM32 embedded hardware. The simulations using Matlab and Multisim were also completed. In [22], a novel class of hyperjerk chaotic systems exhibiting megastability is introduced. Using the Lyapunov spectrum and bifurcation diagrams, different dynamical behaviors of one of the proposed systems are examined. For one of the suggested systems, PSpice simulation

and PIC18F microcontroller realization are performed. An FO 3D system derived from a modified Chua's circuit system is introduced in [23]. Bifurcation analysis, multistability, and coexisting attractors are investigated. A microcontroller-based 3D FO system was implemented with an Arduino UNO board. In addition, PSpice simulations are done. Reference [24] introduces a novel 4D autonomous hyperchaotic system that is built upon the 3D chaotic system described in [25]. Numerical and analytical studies of the dynamic properties are investigated. The LEs are calculated. The presented system is simulated and implemented using a Proteus circuit simulator. In addition, two external digital-to-analog converters (DACs) and a 16-bit dsPIC microcontroller are utilized to operate the system. An autonomous chaotic system in 3D is introduced in [25]. This system produces a chaotic attractor through the changing of two parameters. The dynamic properties were investigated analytically and numerically through the utilization of an electronic circuit consisting of operational amplifiers (OAs). Its microcontroller-based realization was implemented with the PIC32 and external DACs. In [26], a 3D chaotic system with five terms is introduced. The MATLAB/Simulink program uses numerical simulations to demonstrate how the system is synchronized. The secure communication implementation is done on the STM32 development board. The dynamical behaviors of the suggested system, including equilibria, bifurcation, phase plains, time series, and LE, are analyzed. A chaotic 3D attractor with seven terms involving a line and unstable equilibria is proposed in [27]. A comprehensive analysis is conducted on the intricate dynamical behavior of the system through the examination of its equilibria, LE, and bifurcation diagram. Analog circuit implementation and numerical and PSpice simulations are utilized to analyze the periodic states of the system. The realization of the system is performed utilizing an STM32 microcontroller. A 4D chaotic system is developed, and its dynamic behaviors are examined in Reference [28]. The system is implemented using analog active components and validated using PSpice simulation. The C8051 8-bit microcontroller-based random number generator, which uses the proposed chaotic system is designed. The comparison of the chaotic systems using the embedded microcontrollers in the literature with the present hyperchaotic system in this work is shown in Table 1.

As seen in Table 1, some of the chaotic circuits using microcontrollers proposed in the literature are 3D implementations [23], [25] – [27]. Some of these circuits do not exhibit hyperchaotic behavior [22], [23], 25 - 28]. They contain a limited number of non-linear terms [22] – [25], [28] and a smaller number of variable parameters [22], [26], [27]. Chaos applications have been implemented using low bit size microcontrollers [22], [23], [28]. It can be concluded that the hyperchaotic system presented in this work is advantageous compared to similar studies proposed in the literature.

The main goal of path planning research is to construct an AMR system that can completely cover any environment containing dynamic or static obstacles at a given time. Due to the unpredictable nature of chaos, chaotic systems are one of the methods used in path planning. In the literature, studies on chaotic path planning using various chaotic equations such as Lorenz, Chen, and Chua have been presented [29]-[36].

We introduce a new 4D hyperchaotic system in this paper. Dynamic properties such as chaotic attractors, equilibrium point stability, spectrum of LE, and bifurcation diagrams are examined in the suggested hyperchaotic system. The 4D hyperchaotic system is validated using embedded hardware (STM32 microcontrollers) and MATLAB simulations. A path planning application example is provided in the form of an AMR controlled by the proposed hyperchaotic system.

**Table 1:** The comparison of the chaotic systems implemented with the microcontroller.

| Ref. | Dimension of system | Type of system | Number of non-linear terms | Number of variable parameters | Used MC | Bit size of MC |
|---|---|---|---|---|---|---|
| [21] | 4D | Hyperchaotic | 3 quadratic terms | 4 | STM32 | 32-bit |
| [22] | 4D | Chaotic | 1 sinusoidal term | 1 | PIC18F | 8-bit |
| [23] | 3D | Chaotic | 1 quadratic term | 4 | Arduino UNO | 8-bit |
| [24] | 4D | Hyperchaotic | 2 quadratic terms | 4 | dsPIC33FJ | 32-bit |
| [25] | 3D | Chaotic | 2 quadratic terms | 4 | PIC32 | 32-bit |
| [26] | 3D | Chaotic | 2 quadratic terms and 1 cubic term | 1 | STM32 | 32-bit |
| [27] | 3D | Chaotic | 5 quadratic terms | 2 | STM32 | 32-bit |
| [28] | 4D | Chaotic | 2 cubic terms | 5 | C8051 | 8-bit |
| Prop. | 4D | Hyperchaotic | 4 quadratic terms | 7 | STM32 | 32-bit |

MC: Microcontroller

## 2 Novel 4D hyperchaotic system and its analysis

A novel autonomous hyperchaotic system with 4 dimensions, 7 parameters, and 4 quadratic non-linear terms are given below:

$$\dot{x} = ay - bx \tag{1a}$$

$$\dot{y} = cxz \tag{1b}$$

$$\dot{z} = d - exy \tag{1c}$$

$$\dot{u} = fy^2 - gu^2 \tag{1d}$$

where x, y, z, and u are the state variables, and a, b, c, d, e, f, and g are the positive constant parameters. For the presented hyperchaotic system, the initial values of the state parameters and the constant parameters are selected as (*x, y, z, u*) = (5.5, 2.8, 0.3, 0.1) and (*a, b, c, d, e, f, g*) = (4.8, 3, 0.8, 5.5, 1, 1.2, 2.58), respectively. The equilibrium points are calculated as follows:

$$E_{1,2}(x,y,z,u) = \left( \pm\sqrt{\frac{ad}{be}}, \pm\sqrt{\frac{bd}{ae}}, 0, \pm\sqrt{\frac{bdf}{aeg}} \right) \tag{2}$$

To examine the stability, the Jacobian matrix is obtained. For this, the differential equations of the system must be differentiated for each variable. Accordingly, the matrix is found as follows:

$$J = \begin{pmatrix} -b & a & 0 & 0 \\ cz & 0 & cx & 0 \\ -ey & -ex & 0 & 0 \\ 0 & 2fy & 0 & -2gu \end{pmatrix} \tag{3}$$

After the equilibrium points, $E_1$ and $E_2$, found are substituted in the Jacobian matrix, and it is calculated as in Equation (4):

$$J_{1,2} = \begin{pmatrix} -b & a & 0 & 0 \\ 0 & 0 & \pm c\sqrt{\frac{ad}{be}} & 0 \\ \mp\sqrt{\frac{bde}{a}} & \mp\sqrt{\frac{ade}{b}} & 0 & 0 \\ 0 & \pm 2f\sqrt{\frac{bd}{ae}} & 0 & \mp 2\sqrt{\frac{bdfg}{ae}} \end{pmatrix} \tag{4}$$

**Table 2:** Eigenvalues for both equilibrium points.

| Equilibrium point | $\lambda_1$ | $\lambda_2$ | $\lambda_3$ | $\lambda_4$ |
|---|---|---|---|---|
| $E_1$ | -6.5246 | -3.9370 | 0.4685 + j3.2418 | 0.4685 - j3.2418 |
| $E_2$ | 6.5246 | -3.9370 | 0.4685 + j3.2418 | 0.4685 - j3.2418 |

The characteristic equations of the system are found by using the matrix found as det (*J* - *λI*), where the matrix I is a 4x4 diagonal unit matrix. Equation (5a) and (5b) are obtained for the equilibrium points $E_1$ and $E_2$, respectively.

$$\begin{aligned} \det(J_1 - \lambda I) = {} & \lambda^4 + \left( b + 2\sqrt{\frac{bdfg}{ae}} \right)\lambda^3 + \\ & + \left( \frac{acd}{b} + 2b\sqrt{\frac{bdfg}{ae}} \right)\lambda^2 + \\ & + 2cd\left( a + \sqrt{\frac{adfg}{be}} \right)\lambda + 4cd\sqrt{\frac{abdfg}{e}} \end{aligned} \tag{5a}$$

$$\begin{aligned} \det(J_2 - \lambda I) = {} & \lambda^4 + \left( b - 2\sqrt{\frac{bdfg}{ae}} \right)\lambda^3 + \\ & + \left( \frac{cad}{b} - 2b\sqrt{\frac{bdfg}{ae}} \right)\lambda^2 + \\ & + 2cd\left( a - \sqrt{\frac{adfg}{be}} \right)\lambda - 4cd\sqrt{\frac{abdfg}{e}} \end{aligned} \tag{5b}$$

Here, in this study, $a > 0$, $b > 0$, $c > 0$, $d > 0$, $e > 0$, $f > 0$ and $g > 0$ are taken. For both equilibrium points, roots of the characteristic equation are obtained in two different regions of the complex domain. For the first equilibrium point $E_1$, $\lambda_1$ and $\lambda_2$ are obtained as negative real numbers. The other roots $\lambda_3$ and $\lambda_4$ are obtained as two complex numbers that conjugate with each other. These complex numbers have a positive real part. For the second equilibrium point $E_2$, $\lambda_1$ and $\lambda_2$ are obtained as positive and negative real numbers, respectively. As in the $E_1$, $\lambda_3$ and $\lambda_4$ eigenvalues are obtained as the same complex numbers. Hence, this hyperchaotic system is unstable. In Table 2, the calculated eigenvalues for both equilibrium points are given.

Figure 1 illustrates the LE of the suggested 4D hyperchaotic system in time. When the LE of the proposed system are calculated with these values, the values obtained are $L_1$ = 0.5168, $L_2$ = 0.0155, $L_3$ = -3.5305, and $L_4$ = -6.9981 [37]. Here, the positive maximum LE confirms the chaotic nature of the signals produced. If the Kaplan-Yorke Dimension of the proposed 4D hypercha-

otic system is founded using these exponents according to Equation (6), 2.1507 is obtained [38], when j is the maximum index to provide $\sum_{i=1}^{j} K_i > 0$ , by arranging the exponents descending order as $L_1 > L_2 > \ldots > L_n$.

$$D_{KY} = j + \frac{\sum_{i=1}^{j} L_i}{\left|L_{j+1}\right|} \tag{6}$$

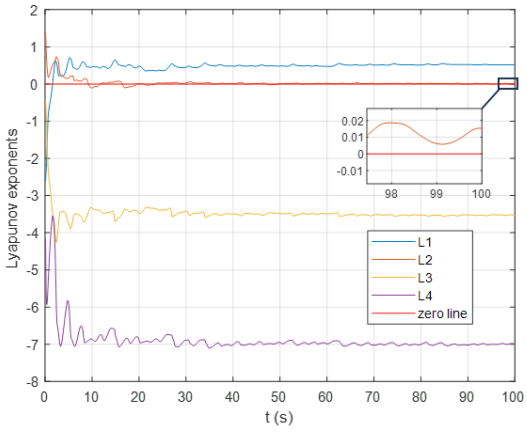


**Figure 1:** Lyapunov exponents of the system in time.

Furthermore, the Jacobian matrix for the suggested system is used to obtain the divergence value ΔV value, which determines the dissipativity of the system. If this ΔV value is negative, the system exhibits chaotic attractors and chaotic behavior under specified beginning conditions. The divergence value of the system is – 9.5245689. Since $\Delta V < 0$, the system behaves chaotically.

**Table 3:** The parameter region showing chaotic behavior.

| Parameters | Parameter Range of Chaotic Behavior | Parameter Range of Hyperchaotic Behavior |
|---|---|---|
| a | 0 < a < 14.2<br>15.6 < a < 20 | 4.2 < a < 5<br>9.1 < a < 14.5<br>15.6 < a < 20 |
| b | 0 < b <20 | 1.7 < b <3.2 |
| c | 0.3 < c < 5.2<br>5.8 < c < 12.8<br>13.9 < c < 20 | 0.4 < c <1.4<br>2.4 < c < 5.2 |
| d | 1.0 < d < 1.6<br>1.9 < d < 20 | 7.5 < d < 8.3<br>9.6 < d < 16.9 |
| e | 0 < e < 20 | 1.5 < e < 3<br>5.3 < e < 5.9 |
| f | 0 < f < 20 | 0.8 < f < 1.4<br>13.8 < f < 15.9 |
| g | 0 < g < 20 | 2 < g < 2.7<br>6.7 < g < 7.4 |

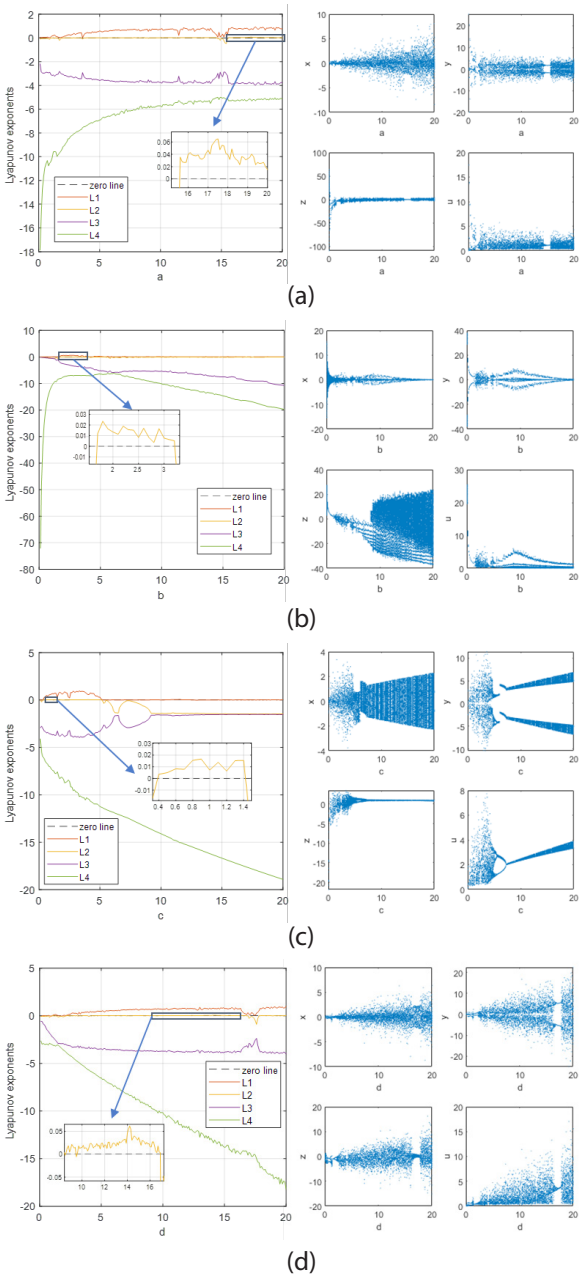


**Figure 2:** Lyapunov exponents and bifurcation diagrams of the system.

Lyapunov exponents and bifurcation diagrams of the suggested system according to the a, b, c, and d parameter values are also given in Figure 2. Table 3 illustrates the regions where the proposed chaotic system shows chaotic and/or hyperchaotic behavior according to its parameters. These ranges are obtained from the LE diagrams in Figure 2, and Table 3 shows the ranges in which certain parameters exhibit chaotic and hyperchaotic behavior. These ranges are crucial for understanding the dynamic properties of the system. When the initial values and constant parameters given above were applied to the hyperchaotic system given by Equation

(1), the Lyapunov spectra seen in Figure 1, the LEs and the bifurcation diagrams seen in Figure 2 and Table 3 were examined, and it was determined that the system showed chaotic behavior for a very wide range of values. Parameter *a* exhibits a wide range of chaotic behavior with distinct intervals interspersed with non-chaotic regions. For the parameter *a*, chaotic behavior is observed in the ranges 0 to 14.2 and 15.6 to 20. The parameter *a* shows hyperchaotic behavior in the ranges 4.2 to 5, 9.1 to 14.5 and 15.6 to 20. Parameter *b* exhibits continuous chaotic behavior between 0 and 20, while hyperchaotic behavior occurs in the range 1.7 to 3.2.

The parameter *c* exhibits chaotic behavior in two distinct intervals and hyperchaotic behavior in one interval. Parameters *d*, *e*, and *g* show similar patterns of chaotic and hyperchaotic behavior over multiple intervals. Interestingly, parameter *f* exhibits a continuous range of chaotic behavior, with no hyperchaotic regions within the given parameter range. Overall, the dynamics of the system appear to be highly sensitive to parameter changes, particularly for parameters *a*, *c*, *d*, and *g*. This sensitivity is evident from the distinct intervals of chaotic and hyperchaotic behavior observed for these parameters. Further analysis using mathematical tools such as Lyapunov exponents could provide more detailed insights into the dynamics of the system and the transitions between chaotic and hyperchaotic regimes.

Based on the above-mentioned findings, it can be said that the system parameter values that put the system into chaotic behavior are in a wide range. In this way, if the system parameters are selected at appropriate values during an application, the proposed 4D hyperchaotic system will show chaotic behavior without being affected much by the tolerances or deviations of the circuit components and power supplies to be used in the application.

## 3 Simulation and experimental results

The system in (1) were defined in the MATLAB program, and the changes with time of the state variables were obtained for (*a, b, c, d, e, f, g*) = (4.8, 3, 0.8, 5.5, 1, 1.2, 2.58) values. The results obtained are given in Figure 3.

The changes of the variables relative to each other were also plotted with the MATLAB program for the same (*a, b, c, d, e, f, g*) values. Figure 4 shows the plots of the changes of the variables over time relative to each other in the following order: x-y variables in (a), x-u variables in (b), x-z variables in (c), y-z variables in (d), y-u variables in (e), u-z variables in (f), x-y-u variables in (g), x-y-z variables in (h), z-u-x variables in (i), and y-z-u variables in (j).

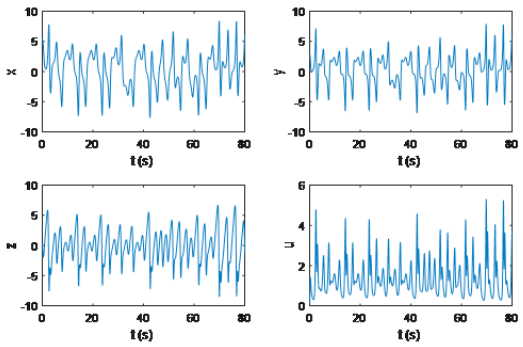


**Figure 3:** MATLAB results for state variables.

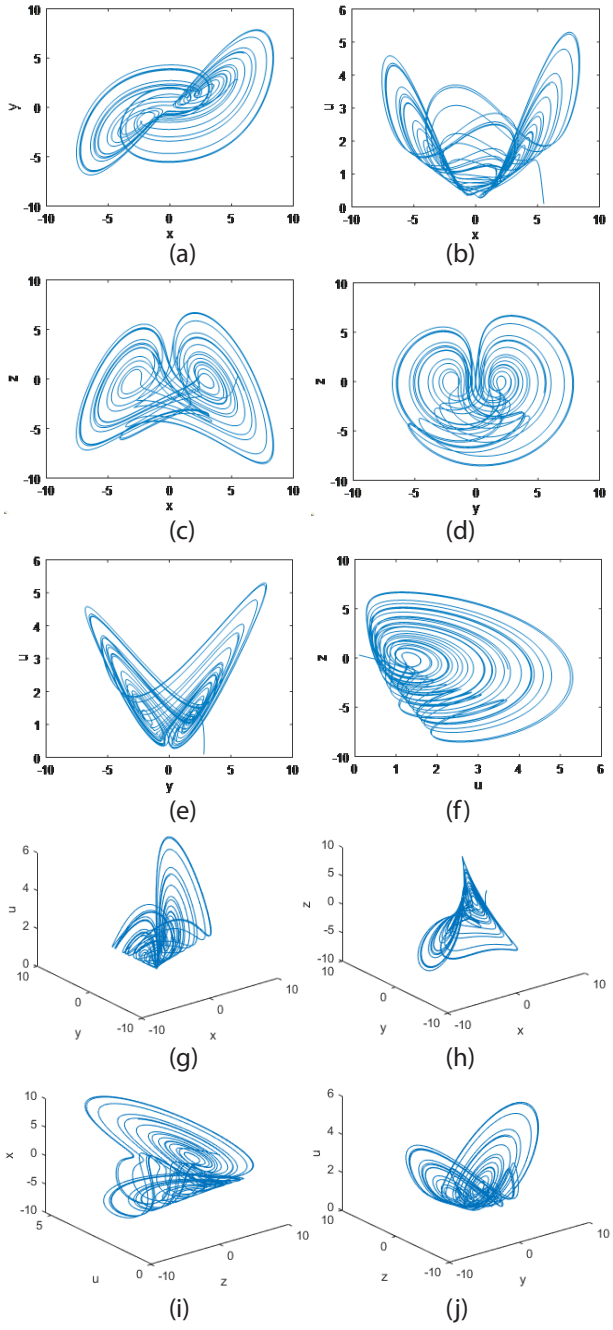


**Figure 4:** Change of state variables relative to each other.

After obtaining the ideal responses of the system through simulation processes, the system was also physically realized. For this, the electrical signals of the state variables were produced using the STM32 microcontroller. First, two separate DAC outputs were set from the STM32 settings. Then, the system state variables are defined in the coding section. When the ideal signals obtained with MATLAB were examined, it was observed that negative values were also obtained. At the same time, values higher than the voltage value that the microcontroller can provide were observed. Since the values for these two cases cannot be obtained with the microcontroller, the obtained values are normalized to be between 0 V and 3.3 V. The algorithm diagram of the written code is given in Figure 5.

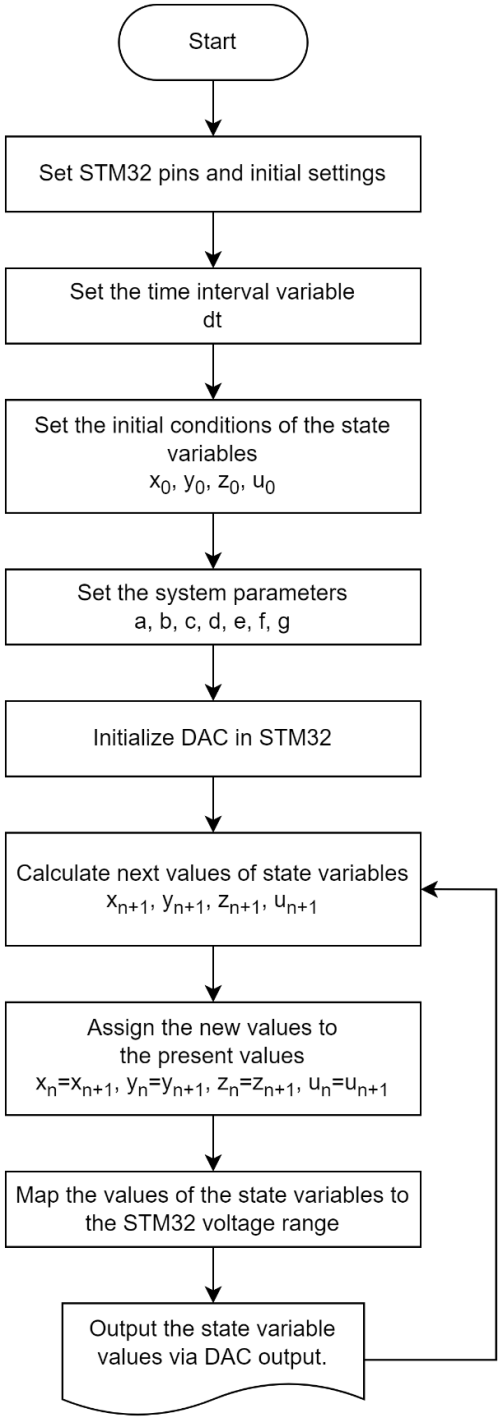


**Figure 5:** The flow chart of the microcontroller program.

The time variation of the signals produced by the microcontroller was measured and displayed with an oscilloscope. The oscilloscope results of the variables x in Figure 6 (a), y in Figure 6 (b), z in Figure 6 (c), and u in Figure 6 (d) have been added.

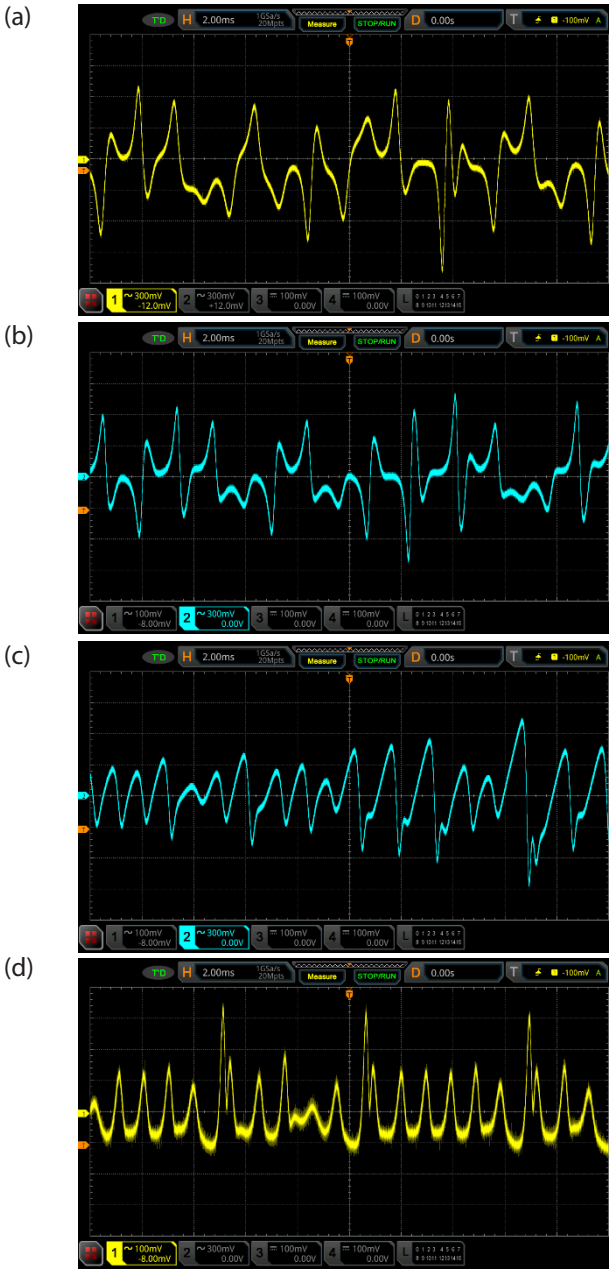


**Figure 6:** Change of state variable signals obtained from the microcontroller over time, (a) x state, (b) y state, (c) z state, and (d) u state.

As in the simulation steps, the changes between the signals obtained with the microcontroller were also observed using the XY mode on the oscilloscope. The obtained results are given in Figure 7. The measured state variable signals relative to each other are in the following order: x-y variables in (a), x-u variables in (b), x-z variables in (c), y-z variables in (d), y-u variables in (e), and u-z variables in (f).

## *4 Chaos-driven autonomous mobile robot application*

Chaotic path planners use chaotic dynamical systems to generate paths within an environment. Path planners are critical for surveillance efforts involving hostile agents, as they require unusual routes and comprehensive coverage of the area. When exploring unknown terrain online, chaotic path planning algorithms can be used without relying on an environmental map. These methods give the designer greater control over the paths generated than random walk algorithms [31]. Recently, many researchers have applied chaotic complex systems to mobile robots [29]-[36]. They have been used in many applications, such as mobile robot patrols, cleaning robots, and many others. However, the simulated trajectories of robots in most of the existing works in the literature show that their coverage is generally low.

The two active wheels are controlled by linear velocity *v(t)* and angular velocity *ω(t)*, as shown in Figure 8. The nonlinear dynamic response of the mobile robot's motion and steering is determined by two independent actuators of analog DC motors that apply appropriate torques to the right and left wheels of the mobile robot [33].

Eq. (7) defines the position vector of the mobile robot's local reference frame, while the global reference frame is [$X_{axis}$, $Y_{axis}$].

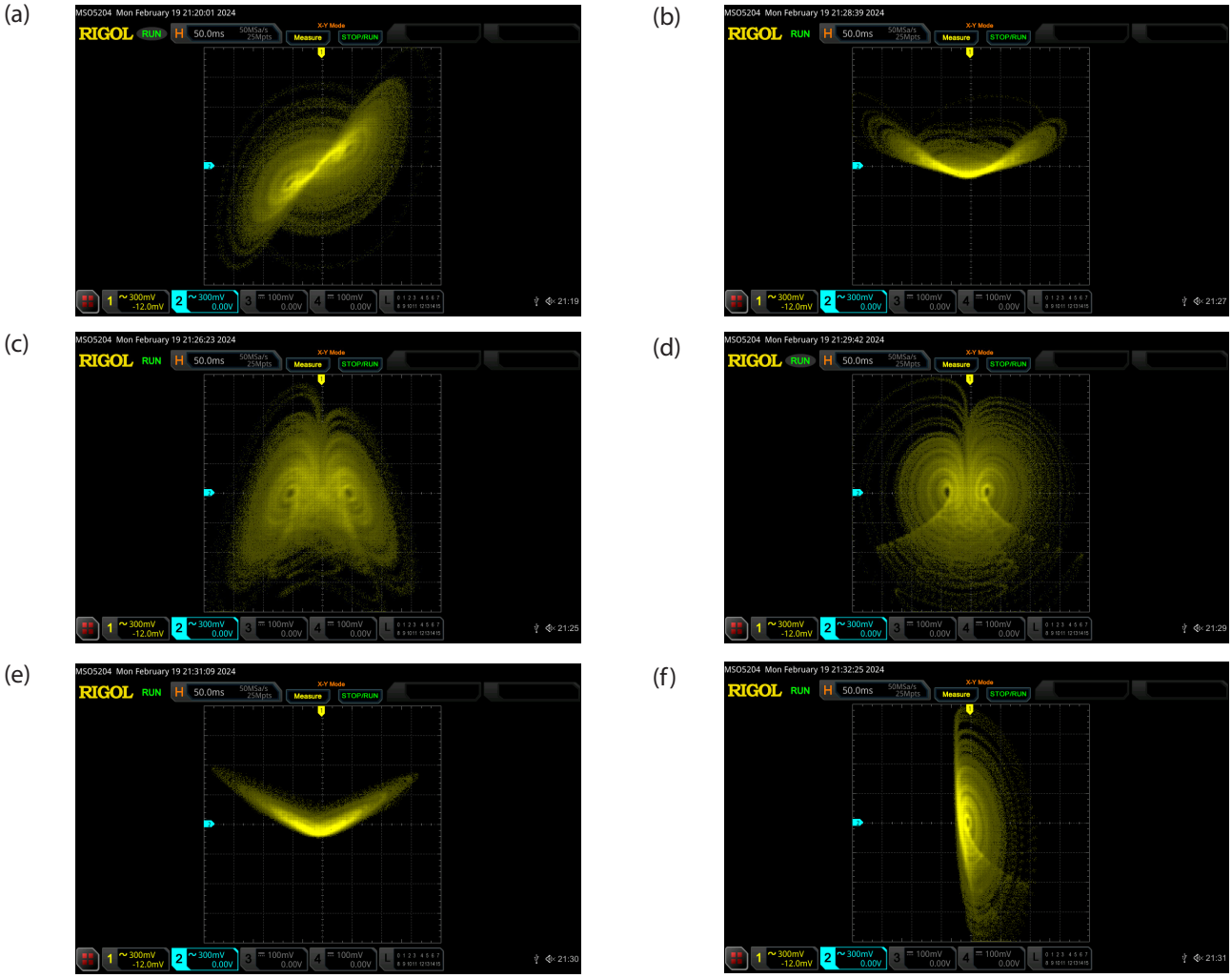


**Figure 7:** Change of state variable signals obtained from the microcontroller to each other, (a) x-y states, (b) x-u states, (c) x-z states, (d) y-z states, (e) y-u states, and (f) u-z states.

$$Q = \left[X_r, Y_r, \theta_r\right]^T \tag{7}$$

Where $X_r(t)$ and $Y_r(t)$ are the position and $\theta_r(t)$ is the orientation of the three-wheeled mobile robot at the midpoint which indicates the location where the left and right wheels meet in the center.

Two primary requirements must be met to confirm the mobile robot's motion and orientation capabilities: each wheel must roll in a pure manner and must not slip for the mobile robot's lateral velocity to equal zero, as stated in Eq. (8).

$$-\dot{X}_r \sin\theta(t) + \dot{Y}_r \cos\theta(t) = 0 \tag{8}$$

As a results, the navigation equation of a three-wheeled mobile robot can be defined as follows [32], [33]:

$$\begin{bmatrix} \dot{X}_r \\ \dot{Y}_r \\ \dot{\theta}_r \end{bmatrix} = \begin{bmatrix} \cos\theta(t) & 0 \\ \sin\theta(t) & 0 \\ 0 & 1 \end{bmatrix} \begin{bmatrix} v(t) \\ \omega(t) \end{bmatrix} \tag{9}$$

where $v(t) = [v_r(t) + v_l(t)]/2$ and $\omega(t) = [v_r(t) - v_l(t)]/L$. The variables $v_r(t)$ and $v_l(t)$ represent the velocity of the right and left wheels, respectively. The direct distance between both wheels is denoted by $L$.

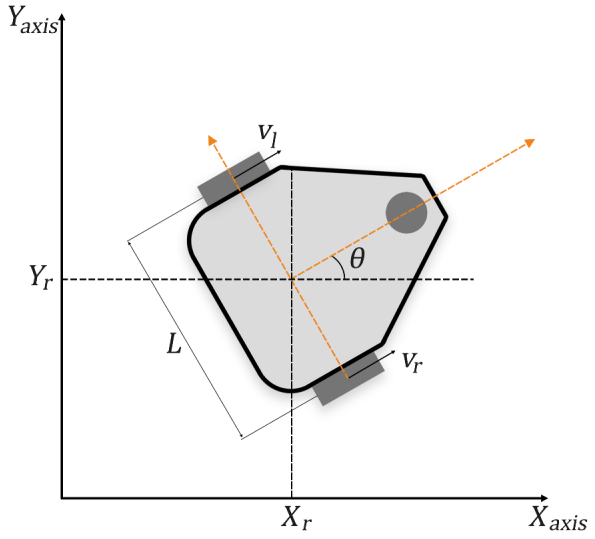


**Figure 8:** Schematic of the three-wheeled AMR navigation

In order to improve the understanding of the robot's chaotic path planning generator, a discontinuous control rule is used, which offers advantages in terms of terrain scanning time. Under this control rule, the robot performs two independent actions. First, to steer the robot directly to the next target coordinate, it rotates around its center with a constant angular velocity $\omega(t)$, as defined by Equation (10). Equation (11), which defines the target, is the path taken by the second action, which is a straight trajectory with constant velocity $v(t)$.

$$\begin{bmatrix} \dot{X}_r \\ \dot{Y}_r \\ \dot{\theta}_r \end{bmatrix} = \begin{bmatrix} 0 \\ 0 \\ \omega(t) \end{bmatrix} \tag{10}$$

$$\begin{bmatrix} \dot{X}_r \\ \dot{Y}_r \\ \dot{\theta}_r \end{bmatrix} = \begin{bmatrix} \cos\theta(t) \\ \sin\theta(t) \\ 0 \end{bmatrix} \tag{11}$$

The idea behind employing a chaotic system for navigation is to substitute two state values from the chaotic equation for the linear velocities of the left and right wheels in the navigation equation. $x(t)$ replaces $v_r(t)$ and $y(t)$ replaces $v_l(t)$. A seven-dimensional system can be created by combining the given hyperchaotic system and the three-wheeled AMR navigation equation in (9).

$$\begin{cases} \dot{x} \\ \dot{y} \\ \dot{z} \\ \dot{u} \\ \dot{X}_r \\ \dot{Y}_r \\ \dot{\theta}_r \end{cases} = \begin{cases} ay - bx \\ cxz \\ d - exy \\ fy^2 - gu^2 \\ \dfrac{x(t)+y(t)}{2}\cos\theta(t) \\ \dfrac{x(t)+y(t)}{2}\sin\theta(t) \\ \dfrac{x(t)-y(t)}{L} \end{cases} \tag{12}$$

Equation (12) shows how the AMR navigates around the suggested hyperchaotic system.

A 20×20 m area is used to test the above equation for robot motion through numerical simulations. The starting position of the mobile robot is ($x$ = 10 $m$, $y$ = 10 $m$) and the system is simulated for 1000, 2000, 3000, and 4000 iterations. Assuming that the limits are located at the horizontal and vertical lines $x$ = 0, $x$ = 21 m, $y$ = 0, $y$ = 21 m. Wheel distance is $L$=0.1 m, initial values of state parameters and constant parameters are chosen as ($x$, $y$, $z$, $u$) = (5.5, 2.8, 0.3, 0.1) and ($a$, $b$, $c$, $d$, $e$, $f$, $g$) = (4.8, 3, 0.8, 5.5, 1, 1.2, 2.58), respectively. As a results, the simulation result generated by MATLAB program the

motion trajectory of the AMR for 1000, 2000, 3000, and 4000 iterations as it is in Figure 9 (a), (b), (c), and (d), respectively.

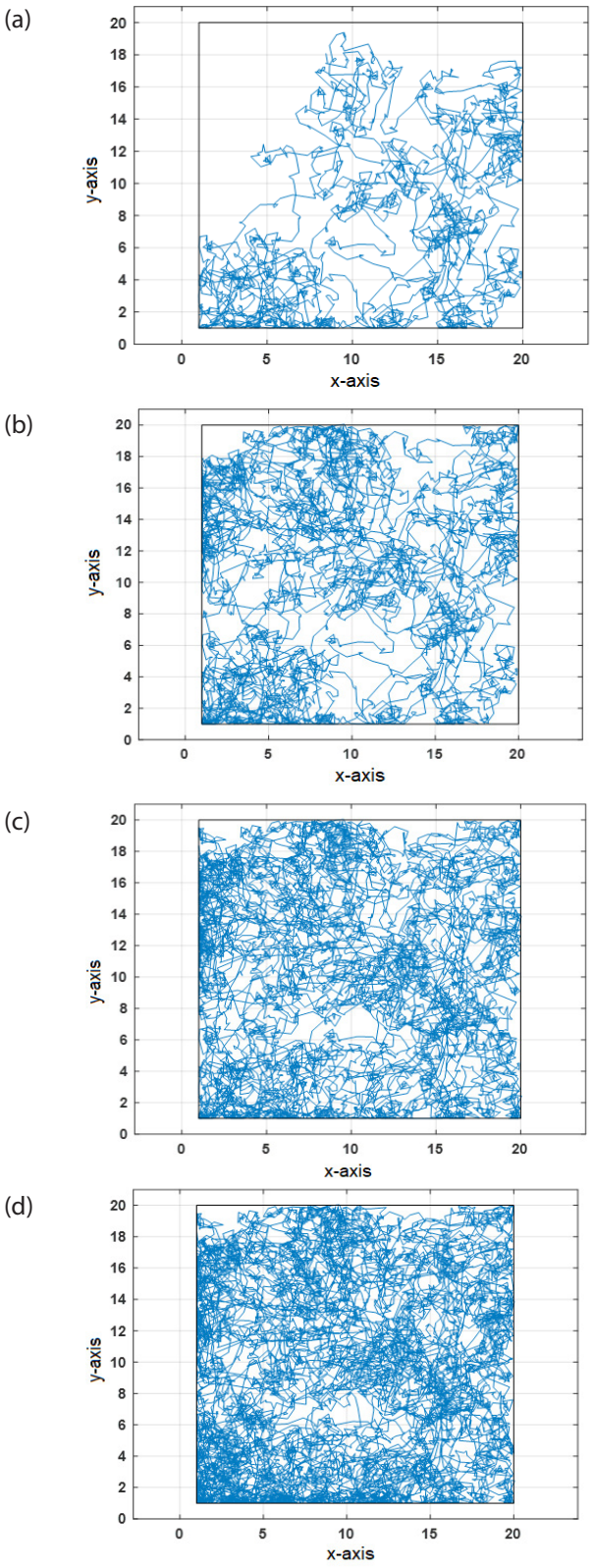


**Figure 9:** Simulation result of navigation path of chaos-driven AMR: a) 1000, b) 2000, c) 3000, d) 4000 iterations.

The above simulations also work for different scenarios in areas of different sizes and shapes. One such scenario is shown in the three simulations in Figure 10. For this, the simulation was repeated by placing a 10×10 m obstacle in the 20×20 m area above. In the simulations, the starting position of the AMR is ($x$ = 10 $m$, $y$ = 10 $m$), the other parameters are chosen as in the previous simulations. The gray areas indicate the obstacles. It is possible to place more than one obstacle of different sizes in different parts of the area.

Simulations with 2000 and 4000 iterations are shown in Figure 10 (a) and (b). As can be seen in Figure 10,

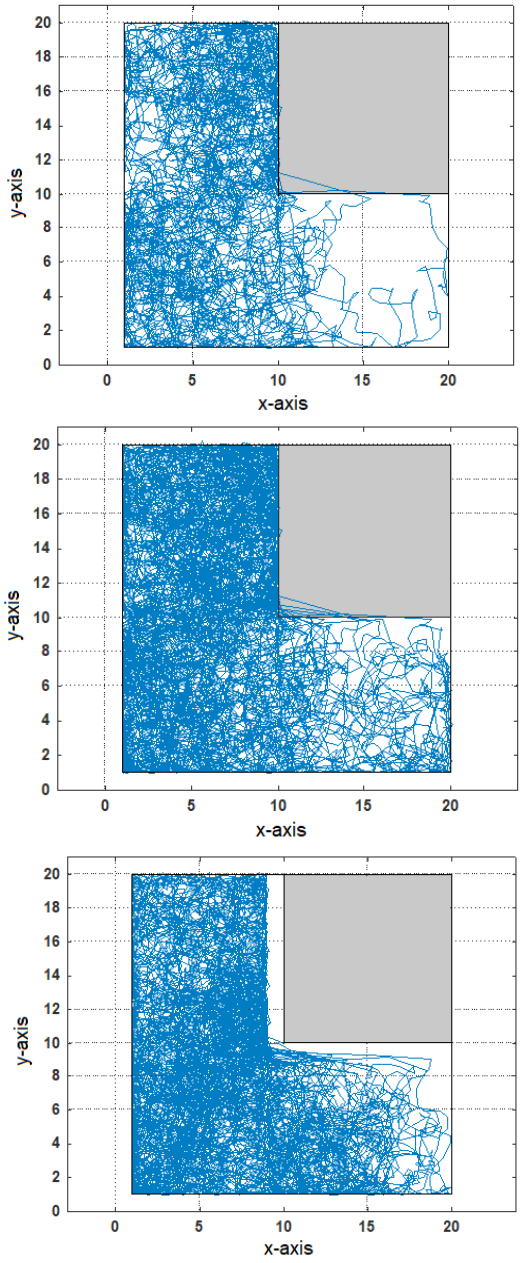


**Figure 10:** Simulation result of the AMR with obstacle: a) 2000, b) 4000, and c) 4000 iterations with 1 m safety distance.

the AMR scanned almost the entire obstacle area as the number of iterations increased. In some cases, the mobile robot entered the obstacle area. To avoid this situation, a robot safety distance can be set. This will prevent the AMR from entering the obstacle area. Another simulation is performed and given as Figure 10 (c), which shows the simulation results of a 20×20 m area with a robot safety distance of 1 m. As can be seen in Figure 10 (c), the AMR is prevented from entering the obstacle area thanks to the safety distance created.

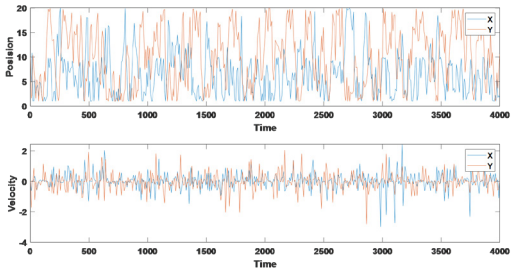


**Figure 11:** Simulation result of the AMR with obstacle: a) Position vs time, b) Velocity vs time graph for 1 m safety distance.

Using acceleration, deceleration, and velocity values of the AMR, a trapezoidal velocity profile trajectory was generated by interpolating waypoints along each dimension (X, Y) using the above parameters in the 20x20 meter with obstacle area [39]. Figure 11 shows the plots the position and velocity with respect to time. As can be seen from Figure 11, the velocity of the AMR varies unpredictably between -2 and +2 m/s depending on the parameters of the proposed hyperchaotic system.

Figure 12 depicts a graph illustrating the average coverage percentage of a specific area by the AMR as a function of the number of iterations. Each iteration is done for one second. Figure 12 presents three distinct curves corresponding to 0.05, 0.1, and 0.2 values of the parameter *L*, representing the wheel distance in meters. For this example, the coverage percentage was achieved at 50% in almost 7900$^{th}$, 4900$^{th}$, and 4300$^{th}$ seconds respectively for the given *L* values. Additionally, when the times for 90% coverage were examined, it was observed that this value was reached at almost 20600$^{th}$, 15600$^{th}$, and 14300$^{th}$ seconds. At the end of this simulation, that is, at the 40000$^{th}$ second, 98.84%, 99.84%, and 99.74% of the 20×20 m area was covered by AMR for each wheel distance, respectively. The number of iterations of the robot increases the coverage percentage also increases. This shows that the AMR scans the area more thoroughly over time, leaving fewer gaps. As the *L* wheel distance increases, more area is scanned in each second and the coverage percentage increases faster.

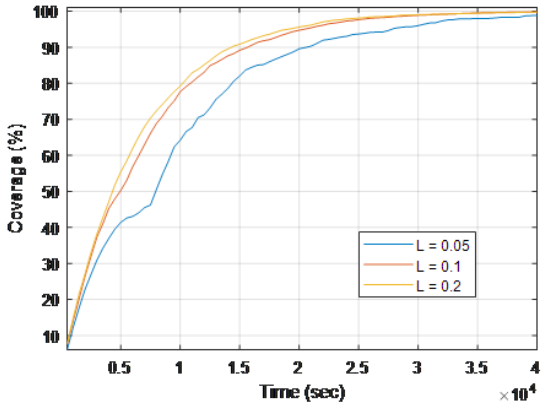


**Figure 12:** Coverage performance of the AMR

## 5 Statistical evaluation of randomness

In order for the proposed hyperchaotic system to be used in various applications, such as cryptography, it must be tested using statistical tests that require long bitstreams of random binary bits. The National Institute of Standards and Technology (NIST) widely uses the NIST SP800-22 test set [40].

We first quantized the values from the chaotic system to prepare the data for testing. We determined the amount of shift to apply to the variables based on their current values in order to increase randomness. For instance, we apply a shift operation in the form of $2^{32}/x[n]$ to shift the variable *x*. We provide the procedures used to prepare the test data below:

Step 1: x, y, z and u variables were converted to 32 bits.
Step 2: The variable y was shifted and XORed with the variable x.
Step 3: The z variable was shifted and XORed with the y variable.
Step 4: The values obtained in steps 2 and 3 were XORed.
Step 5: The variable u was shifted and XORed with the variable z.
Step 6: The variable u is shifted and XORed with the variable x.
Step 7: The results of steps 5 and 6 were XORed.
Step 8: The most significant 16 bits of the result obtained in step 4 and the least significant 16 bits of the result obtained in step 7 were combined.
Step 9: The least significant 16 bits of the result obtained in step 4 and the least significant 16 bits of the result obtained in step 7 were combined.
Step 10: The results obtained in steps 8 and 9 were XORed.

After data preparation, we obtained approximately 14 Mbits. We tested the data for randomness using the NIST 800-22 test tool. There are a total of 15 tests in the NIST 800-22 test suite, and the parameters of each test are described in detail in [40]. For each test to be considered successful, the p-value must be greater than 0.001. The parameters used in the test are shown in Table 4, and the results are shown in Table 5. As seen in Table 5, all standard tests are passed and the test results indicate that the proposed hyperchaotic system exhibits strong randomness properties suitable for secure applications, such as autonomous mobile robot path planning.

**Table 4:** NIST 800-22 test parameters

| Parameter Name | Value |
|---|---|
| Block Frequency Test - block length (M) | 12 |
| Non-Overlapping Template Test - block length (m) | 9 |
| Overlapping Template Test - block length (m) | 9 |
| Approximate Entropy Test - block length (m) | 10 |
| Serial Test - block length (m) | 16 |
| Linear Complexity Test - block length (M) | 50 |

**Table 5:** Microcontroller-based 4D hyperchaotic system NIST 800-22 test results

| Test | p-value | Proportion | Result |
|---|---|---|---|
| Frequency | 0.911413 | 10/10 | Passed |
| Block Frequency | 0.534146 | 8/10 | Passed |
| Cumulative Sums 1 | 0.350485 | 10/10 | Passed |
| Cumulative Sums 2 | 0.739918 | 10/10 | Passed |
| Runs | 0.534146 | 10/10 | Passed |
| Longest Run | 0.534146 | 10/10 | Passed |
| Rank | 0.035174 | 10/10 | Passed |
| FFT | 0.534146 | 10/10 | Passed |
| Non-overlapping Template* | 0.474107 | 10/10 | Passed |
| Overlapping Template | 0.911413 | 10/10 | Passed |
| Universal | 0.739918 | 9/10 | Passed |
| Approximate Entropy | 0.739918 | 10/10 | Passed |
| Serial 1 | 0.739918 | 10/10 | Passed |
| Serial 2 | 0.534146 | 9/10 | Passed |
| Linear Complexity | 0.122325 | 10/10 | Passed |

* Average

## 6 Conclusion

In this study, a novel hyperchaotic system was defined and realized with the embedded hardware STM32 microcontroller. A table comparing the microcontroller-based chaotic systems from existing research with the hyperchaotic system introduced in this study is provided. The proposed structure has several benefits when compared to similar structures in existing literature.

The equilibrium points of the system were calculated using the state variable equations, and the stability of the system was investigated with a bifurcation diagram and LE. Then, to examine the ideal changes in time of these variables, their graphs were plotted according to time and relative to each other in the MATLAB environment, and the simulations were carried out. After that, the state variables were generated as electrical signals using the microcontroller. These signals were produced by converting digital signals to analog signals with a microcontroller and were observed on the oscilloscope screen. As a result, the experimental results obtained by the microcontroller-based implementation of the presented hyperchaotic system coincide with the simulation results from MATLAB.

Efficiently and rapidly exploring a given terrain is a critical challenge in path planning research for autonomous mobile robots. Therefore, an application example of a chaotic path planning of the AMR is provided in order to test the presented hyperchaotic system. For these simulations, a 20×20 m area with and without obstacles is used. The effect of the change in wheel distance on area coverage is also examined.

## 7 Credit author statement

Betul Yurdem: Methodology, Software, Writing - Original Draft, Validation, Writing - Reviewing and Editing. Mustafa Furkan Aksu: Writing - Original Draft, Validation, Writing - Reviewing and Editing. Mehmet Sagbas: Writing - Original Draft, Validation, Writing - Reviewing and Editing.

## 8 Declaration of competing interest

The authors declare that they have no known competing financial interests or personal relationships that could have appeared to influence the work reported in this paper.

## 9 Declaration of generative AI and AI-assisted technologies in the writing process

During the preparation of this work the authors used generative AI in order to improve language and read-

ability. After using this tool/service, the authors reviewed and edited the content as needed and took full responsibility for the content of the publication.

## 10 Data availability

Data sharing is not applicable to this article as no datasets were generated or analysed during the current study.

## 11 Conflict of interest

The authors declare that they have no conflict of interest.

## 12 References


1. J. Gleick and R. C. Hilborn, "Chaos, making a new science," American Journal of Physics, 56, 1053–1054, 1988. https://doi.org/10.1119/1.15345
2. G. Chen, X. Dong, From chaos to order-perspectives and methodologies in controlling chaotic nonlinear dynamical systems, Int. J. Birfuc. Chaos. 3 (6) (1993) 1363–1409. https://doi.org/10.1142/S0218127493001112
3. P.C. Rech, H.A. Albuquerque, A hyperchaotic Chua system, Int. J. Bifurc. Chaos. 19 (2009) 3823–3828. https://doi.org/10.1142/S0218127409025146
4. X. Luo, M. Small, M. Danca, G. Chen, On a dynamical system with multiple chaotic attractors, Int. J. Birfuc. Chaos. 17 (2007) 3235–3251. https://doi.org/10.1142/S0218127407018993
5. O.E. Rössler, An equation for continuous chaos, Phys. Lett. A 57 (5) (1976) 397–398.
6. Q. M. Zainel, S. M. Darwish, and M. B. Khorsheed, "Employing quantum fruit fly optimization algorithm for solving three-dimensional chaotic equations," Mathematics 10(21), 4147 (2022). https://doi.org/10.3390/math10214147
7. Y. Ma and W. Li, "Application and research of fractional differential equations in dynamic analysis of supply chain financial chaotic system," Chaos, Solitons Fractals 130, 109417 (2020). https://doi.org/10.1016/j.chaos.2019.109417
8. L. Wang, "3-scroll and 4-scroll chaotic attractors generated from a new 3-D quadratic autonomous system," Nonlinear Dynamics, vol. 56, no. 4, pp. 453–462, 2009. https://doi.org/10.1007/s11071-008-9417-4
9. B. Bao, J. Xu, Z. Liu, and Z. Ma, "Hyperchaos from an augmented Lu system," International Journal of Bifurcation and Chaos, vol. 20, no. 11, pp. 3689–3698, 2010. https://doi.org/10.1142/S0218127410027969
10. J. Kengne, Z. T. Njitacke, H. B. Fotsin et al., "Dynamical analysis of a simple autonomous jerk system with multiple attractors," Nonlinear Dynamics, vol. 83, no. 1-2, pp. 751–765, 2016. https://doi.org/10.1007/s11071-015-2364-y
11. G. Qi, S. Du, G. Chen, Z. Chen, Z. Yuan, On a four-dimensional chaotic system, Chaos Solitons Fractals 23 (2005) 1671. https://doi.org/10.1016/j.chaos.2004.06.054
12. Qi GY, Chen GR (2006) Analysis and circuit implementation of a new 4D chaotic system. Phys Lett A 352: 386–397. https://doi.org/10.1016/j.physleta.2005.12.030
13. Alshekly, T.K., Albahrani, E.A. & Lafta, S.H. 4D chaotic system as random Substitution-Box. Multimed Tools Appl 81, 15793–15814 (2022). https://doi.org/10.1007/s11042-022-11928-x
14. Jian Ma, Zengqiang Chen, Zhonglin Wang, Qing Zhang, A four-wing hyper-chaotic attractor generated from a 4-D memristive system with a line equilibrium, Nonlinear Dyn (2015) 81:1275–1288, https://doi.org/10.1007/s11071-015-2067-4
15. M. Ababneh, A new four-dimensional chaotic attractor, Ain Shams Engineering Journal 9 (2018) 1849–1854. https://doi.org/10.1016/j.asej.2016.08.020
16. Z. Lingmei, A novel 4-D butterfly hyperchaotic system, Optik, Volume 131, February 2017, Pages 215-220, https://doi.org/10.1016/j.ijleo.2016.11.083
17. F. Yu, S. Xu, X. Xiao, W. Yao, Y. Huang, S. Cai, B. Yin, Y. Li, Dynamics analysis, FPGA realization and image encryption application of a 5D memristive exponential hyperchaotic system. Integration 90, 58–70. https://doi.org/10.1016/j.vlsi.2023.01.006 (2023).
18. Yu F, Zhang W, Xiao X, Yao W, Cai S, Zhang J, Wang C, Li Y. Dynamic Analysis and FPGA Implementation of a New, Simple 5D Memristive Hyperchaotic Sprott-C System. Mathematics. 2023; 11(3):701. https://doi.org/10.3390/math11030701
19. Vaidyanathan, S., Tlelo-Cuautle, E., Sambas, A., Dolvis, L. G. & Guillén-Fernández, O. FPGA design and circuit implementation of a new four-dimensional multistable hyperchaotic system with coexisting attractors. Int. J. Comput. Appl. Technol. 64, 223–234. https://doi.org/10.1504/IJCAT.2020.111848 (2020).
20. Prakash, P., Rajagopal, K., Koyuncu, I. et al. A Novel Simple 4-D Hyperchaotic System with a Saddle-Point Index-2 Equilibrium Point and Multistability: Design and FPGA-Based Applications. Circuits Syst Signal Process 39, 4259–4280 (2020). https://doi.org/10.1007/s00034-020-01367-0

21. Fu, S., Cheng, X. & Liu, J. Dynamics, circuit design, feedback control of a new hyperchaotic system and its application in audio encryption. Sci Rep 13, 19385 (2023). https://doi.org/10.1038/s41598-023-46161-5
22. R. Karthikeyan, S. Çiçek, V.T. Pham, A. Akgul, P. Duraisamy, A class of unexcited hyperjerk systems with megastability and its analog and microcontroller-based embedded system design, Physica Scripta, 95, 055214, 2020. https://doi.org/10.1088/1402-4896/ab7851
23. Wang J, Xiao L, Rajagopal K, Akgul A, Cicek S, Aricioglu B. Fractional-Order Analysis of Modified Chua's Circuit System with the Smooth Degree of 3 and Its Microcontroller-Based Implementation with Analog Circuit Design. Symmetry. 2021; 13(2):340. https://doi.org/10.3390/sym13020340
24. Méndez-Ramírez RD, Arellano-Delgado A, Murillo-Escobar MA, Cruz-Hernández C. A New 4D Hyperchaotic System and Its Analog and Digital Implementation. Electronics. 2021; 10(15):1793. https://doi.org/10.3390/electronics10151793
25. Méndez-Ramírez, R.; Cruz-Hernández, C.; Arellano-Delgado, A.; Martínez-Clark, R. A new simple chaotic Lorenz-type system and its digital realization using a TFT touch-screen display embedded system. Complexity 2017, 2017, 6820492. https://doi.org/10.1155/2017/6820492
26. A. Gokyildirim, U. E. Kocamaz, Y. Uyaroglu, and H. Calgan, A novel five-term 3D chaotic system with cubic nonlinearity and its microcontroller-based secure communication implementation, AEU-Int. J. Electron. Commun., vol. 160, Feb. 2023, Art. no. 154497. https://doi.org/10.1016/j.aeue.2022.154497
27. A. Gokyildirim, A Novel Chaotic Attractor with a Line and Unstable Equilibria: Dynamics, Circuit Design, and Microcontroller-Based Sliding Mode Control, in IEEE Canadian Journal of Electrical and Computer Engineering, vol. 46, no. 3, pp. 228-236, Summer 2023, https://doi.org/10.1109/ICJECE.2023.3275281.
28. S. Kaçar, Analog circuit and microcontroller based RNG application of a new easy realizable 4D chaotic system, Optik, Volume 127, Issue 20, 2016, Pages 9551-9561. https://doi.org/10.1016/j.ijleo.2016.07.044
29. L. Moysis, E Petavratzis, C. Volos, H. Nistazakis, I. Stouboulos, A chaotic path planning generator based on logistic map and modulo tactics, Robotics and Autonomous Systems, 124, 2020, 103377, ISSN 0921-8890, https://doi.org/10.1016/j.robot.2019.103377.
30. Moysis, L., Volos, C., Pham, VT., El-Latif, A.A.A., Nistazakis, H., Stouboulos, I. (2023). Analysis of a Hyperchaotic System with a Hyperbolic Sinusoidal Nonlinearity and Its Application to Area Exploration Using Multiple Autonomous Robots. In: Volchenkov, D., Luo, A.C.J. (eds) New Perspectives on Nonlinear Dynamics and Complexity. Nonlinear Systems and Complexity, vol 35. Springer, Cham. https://doi.org/10.1007/978-3-030-97328-5_4
31. F. Ahuraka, P. Mcnamee, Q. Wang, Z. N. Ahmadabadi and J. Hudack, "Chaotic Motion Planning for Mobile Robots: Progress, Challenges, and Opportunities," in IEEE Access, vol. 11, pp. 134917-134939, 2023, https://doi.org/10.1109/ACCESS.2023.3337371.
32. Sambas, A., Vaidyanathan, S., Mamat, M.: A 3D novel jerk chaotic system and its application in secure communication system and mobile robot navigation. Studies in Computational Intelligence, vol. 636, pp. 283–310, (2016) https://doi.org/10.1007/978-3-319-30279-9_12
33. He, H., Cui, Y., Lu, C., Sun, G. (2020). Time Delay Chen System Analysis and Its Application. In: Tan, J. (eds) Advances in Mechanical Design. ICMD 2019. Mechanisms and Machine Science, vol 77. Springer, Singapore. https://doi.org/10.1007/978-981-32-9941-2_17
34. C.K. Volos, I.M. Kyprianidis, I.N. Stouboulos, A chaotic path planning generator for autonomous mobile robots, Robotics and Autonomous Systems, Vol. 60(4), 2012, pp. 651-656, https://doi.org/10.1016/j.robot.2012.01.001.
35. C. Pimentel-Romero, J. M. Muñoz-Pacheco, O. Felix-Beltran, L. Gomez-Pavon, and C. K. Volos, Chaotic Planning Paths Generators by Using Performance Surfaces. Cham, Switzerland: Springer, 2017, pp. 805–832. https://doi.org/10.1007/978-3-319-50249-6_28
36. C. Nwachioma and J. H. Pérez-Cruz, "Analysis of a new chaotic system, electronic realization and use in navigation of differential drive mobile robot," Chaos, Solitons Fractals, vol. 144, Mar. 2021, Art. no. 110684. https://doi.org/10.1016/j.chaos.2021.110684
37. A. Wolf, J.B. Swift, H.L. Swinney, J. A. Vastano, Determining Lyapunov exponents from a time series, Physica D: Nonlinear phenomena 16(3), 285-317, 1985. https://doi.org/10.1016/0167-2789(85)90011-9
38. P. Frederickson, J. L. Kaplan, E. D. Yorke and J. A. Yorke, The liapunov dimension of strange attractors, J. Differ. Equations 49(2), 185-207, 1983. https://doi.org/10.1016/0022-0396(83)90011-6.

39. Lynch, Kevin M., and Frank C. Park. Modern Robotics: Mechanics, Planning and Control. Cambridge: Cambridge University Press, 2017.
40. A statistical test suite for random and pseudo random number generators for cryptographic applications; 2010: April [NIST 800–22 Rev 1a]



Arrived: 15. 09. 2024
Accepted: 24 .03. 2025